Distribution of ion energies incident on electrodes in capacitively coupled rf discharges

M. J. Kushner
Spectra Technology, Inc. (Formerly Mathematical Sciences Northwest, Inc.), 2755 Northup Way, Bellevue, Washington 98004

(Received 19 July 1985; accepted for publication 14 August 1985)

The energy and angular distribution of ions striking the electrodes in rf discharges are of interest with respect to the application of such discharges to the processing of semiconductor materials. The ability to fabricate small ($< 1\ \mu$m) semiconductor features using the plasma etching process results, in part, from the energetic and anisotropic flux of ions which strike the semiconductor surface. In this paper the energy and angular distribution of ions striking the electrodes in low-pressure capacitively coupled rf discharges are studied using a Monte Carlo model for ion trajectories and a parametric model for the time-dependent electric field within the sheath. Energy and angular distributions are discussed as a function of rf frequency, ion mass, and the mean-free path between charge exchange collisions within the sheath. The ion energy distribution is found to be characterized by a scaling parameter proportional to (rf frequency $\times$ sheath thickness)^2 $\times$ ion mass/(sheath voltage); small values of this parameter yield bimodal distributions, intermediate values yield distributions peaked at the maximum sheath potential, and high values yield distributions peaked at the average sheath potential. The ion energy distribution is also examined for different values of the dc and rf components of the sheath potential and for different models for the electric field within the sheaths. When the dc component of the sheath potential is small compared to the rf amplitude, a large thermal component to the ion energy distribution results. The implication of this result and that for the angular distribution of ions incident on the electrodes is discussed with respect to the isotropy of the etch obtained during plasma etching of semiconductor materials.

I. INTRODUCTION

In capacitively coupled radio frequency (rf) discharges of the type used for plasma processing of semiconductor materials, the plasma potential, and hence the sheath potential at the electrodes can have a time varying value of tens to hundreds of volts.[1-7] When electrodes of different effective areas are used, the plasma potential can also have a large dc component with respect to one or more of the electrodes.[8,9] A dc component to the plasma potential can also be obtained by applying a dc bias to the excitation electrode. The maximum value of the applied dc or self-bias potential that can be sustained with capacitive coupling to the rf power source is approximately equal to the amplitude of the applied rf voltage.

The sheath potential at an electrode in a capacitively coupled rf discharge is the difference between the potential of that electrode and the plasma potential. At a grounded electrode, the sheath potential is equal to the plasma potential. At a powered electrode, the sheath potential is the difference between the applied (and self-biased) potential and the plasma potential. Large negative sheath potentials result in the electrodes, and the semiconductor materials placed on the electrodes, being bombarded by energetic ions. The ions diffuse or drift out of the plasma and are accelerated through the sheaths at the electrodes into the surface. Because the magnitude of the plasma potential is large compared to the thermal energy of the ions as they drift out of the plasma, and the thickness of the sheaths are large compared to the surface features of the material on the electrodes, ions can be directed perpendicularly to the semiconductor surface after being accelerated through the sheaths. Therefore, horizontal surfaces (i.e., perpendicular to the flux of ions) will be bombarded at a much higher rate than vertical surfaces (i.e., parallel to the flux of ions).

In the plasma etching of semiconductor materials, features with dimensions less than 1 μm can be fabricated.[3] In order to produce such features, etching rates in the vertical direction must exceed those in the horizontal direction by a large factor; that is the etching must be anisotropic. The ability to etch anisotropically in rf discharges results, in part, from the preferential bombardment of horizontal surfaces by the vertically directed flux of ions and the fact that the rate at which the etching reaction takes place is greatly enhanced when the semiconductor surface is bombarded by ions.[3,10-12] The energy and angular distribution of ions striking the semiconductor surface are therefore important in describing details of the etching process.

The power deposited by ions on the surface of a semiconductor is also believed to be important during plasma enhanced chemical vapor deposition (PECVD) of thin films.[13-16] During the deposition of thin films of amorphous hydrogenated silicon from silane plasmas by PECVD, the surface morphology, fraction of hydrogen in the film, optical band gap, and rate of deposition have all been observed to be functions of the magnitude and energy of the impinging ion flux.

The ion energy distribution (IED) and angular distribution (IAD) of ions striking the semiconductor surface during plasma processing are seen to be parameters of great interest in describing the plasma–semiconductor interaction. In this

 0021-8979/85/234024-08$02.40 © 1985 American Institute of Physics

paper, a parametric model for an rf sheath is used in conjunction with a Monte Carlo analysis to obtain these distributions by computing ion trajectories through the oscillating rf sheath. Analytic treatments have previously been used to obtain the IED[4,6] and experimental measurements of the IED have been made.[1,2,5–7] Analytic treatments of the IED have been somewhat constrained by assumptions made in the analysis; the ion transit time is much longer than the rf period,[6] the sheath is collisionless,[4–6] and the electric field in the sheath has a specific form.[4] The Monte Carlo method was chosen here in order to include collisions in the sheath, to enable the use of an arbitrary model for the electric field within the sheath, to examine a wide range of rf frequencies, and to obtain the angular distribution of the ions striking the electrodes.

The sheath and ion trajectory models will be described in Sec. II. Ion energy and angular distributions computed with the model are discussed in Sec. III where we examine the effect of rf frequency, ion mass, dc potential, and collisions within the sheath. A scaling parameter, proportional to the product of (rf frequency × sheath thickness)^2 × ion mass/(sheath potential), is used to characterize the shape of the IED; small values of this parameter result in bimodal distributions, intermediate values result in distributions peaked at the maximum sheath potential, and large values result in distributions peaked at the average sheath potential. Collisions within the sheath thermalize the IED and spread the IAD away from the vertical. A similar effect is observed when the dc sheath potential is small compared to the rf amplitude. The implication of these results for the isotropy of the etch obtained during plasma etching is discussed in Sec. IV. Concluding remarks are in Sec. V.

II. DESCRIPTION OF THE PARAMETRIC SHEATH AND THE MONTE CARLO ION TRAJECTORY MODELS

In this analysis, we will examine a capacitively coupled, parallel plate rf electropositive discharge having a powered electrode and a grounded electrode. The energy distributions we will discuss are for ions striking the powered electrode. Parametric model for the time-dependent plasma potential and sheath thickness are used. These models for the plasma potential and sheath thickness in an electropositive discharge are

$$\phi_P(t) = \mathrm{MAX}(\phi_{dc}^* + \phi_{rf} \sin(\omega_{rf} t), \Delta\phi), \quad (1)$$

$$l(t) = l_{dc} + l_{rf} \sin(\omega_{rf} t + \alpha), \quad (2)$$

where $\phi_P(t)$ is the plasma potential at time t, $l(t)$ is the sheath thickness, and $\Delta\phi$ is a small positive value approximately equal to the floating sheath potential.[17] MAX (a,b) is the maximum value of a and b. The subscripts indicate dc and rf values, and the superscript * indicates an applied (or self-biased) potential. The rf frequency is ω_{rf} and α is the phase difference between the oscillation of sheath thickness and plasma potential. This form of the plasma potential is appropriate for a sheath displaying dominantly resistive behavior.[1] An alternate form of the plasma potential for the sheath displaying dominantly capacitive behavior is discussed in Sec. III D. For capacitively coupled discharges, $|\phi_{dc}^*| \leq \phi_{rf}$.

For electropositive plasmas, the sheath potentials at either electrode generally remain negative at all times (see Sec. III D). The sheath potential at the grounded electrode, $\phi_S(t)$, is negative and equal in magnitude to the plasma potential. The sheath potential at the powered electrode is the difference between the potential of that electrode and the plasma potential

$$\phi_S = \phi_{dc}^* + \phi_{rf}^* \sin(\omega_{rf} t) - \phi_P(t). \quad (3)$$

For this analysis we choose a geometry[1] such that $\phi_{dc}^* < 0$ and assume that the voltage drop between the sheaths is small so that $\phi_{rf}^* \cong \phi_{rf}$. For these conditions the sheath potential at the powered electrode is

$$\phi_S(t) = \mathrm{MIN}[\phi_{dc}^* + \phi_{rf}^* \sin(\omega_{rf} t), -\Delta\phi], \quad (4)$$

where MIN (a,b) is the minimum value of a and b. The plasma potential and sheath potential for resistive sheaths are shown schematically in Fig. 1.

Spatial dependence within the sheath is obtained by specifying a functional dependence for the electric field on position. We use a parametric form for the electric field,

$$E(x,t) = E_0[l(t) - x]^a, \quad E_0 = -\phi_S(t)\frac{(a+1)}{l(t)^{(a+1)}}, \quad (5)$$

where a is positive. With $a = 1$, the electric field decreases in magnitude linearly proportional with distance from the electrode. Recent spectroscopic measurements of electric fields within the sheath of an rf plasma of the type considered here have yielded this linear dependence.[18] Therefore we will use $a = 1$ for the majority of our studies.

Ion trajectories are computed using standard Monte Carlo techniques.[19] Initial velocities are randomly chosen from a Maxwellian distribution and the ions are directed towards the sheath starting at a location greater than the maximum spatial extent of $l(t)$. The ions initially have a randomly selected phase with respect to the rf cycle.

Collisions are included in the analysis. For each ion a mean-free path between collisions is defined by

$$\lambda_{MFP} = (\sigma N)^{-1}, \quad (6)$$

where σ is the total collision cross section and N is the density of collision partners. A collision occurs when traversing a distance Δs if

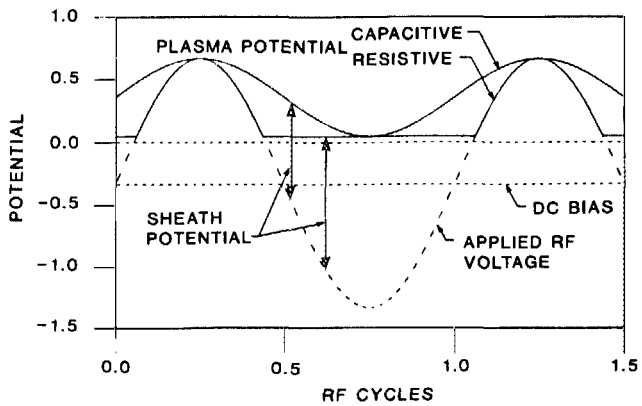

FIG. 1. Schematic of the plasma potentials for sheaths displaying dominantly resistive and capacitive characteristics. In this example, the dc potential of the electrode is −0.33 and the amplitude of the applied rf voltage is 1.0. The instantaneous sheath potential is the difference between the potential of the electrode and the plasma potential.

$$\Delta s \leqslant -\lambda_{\mathrm{MFP}} \ln(r), \tag{7}$$

where r is a randomly distributed number between 0 and 1. We include only charge exchange collisions in the sheath as the cross section for this process is usually large compared to the cross section for elastic collisions between ions and neutrals. In a charge exchange collision, the scattering angle of the new ion with respect to the trajectory of the original ion is isotropic. The energy of the new ion is randomly chosen from a Maxwellian distribution having the neutral gas temperature.

It is convenient to generalize the analysis by expressing variables and parameters in dimensionless form. For this purpose, position is normalized by the Debye length, time is normalized by the plasma frequency period, and the electrical potential and heavy particle temperature (ion or neutral) are normalized by the electron temperature. That is,

$$\tau = \frac{T}{T_e}, \quad \chi = \frac{x}{\lambda_D}, \quad \delta = \frac{t\omega_P}{2\pi}, \quad \psi = \frac{2\pi\nu_{\mathrm{rf}}}{\omega_P}, \tag{8}$$

$$\Phi = \frac{e\phi}{kT_e}, \quad \eta = \frac{eE\lambda_D}{kT_e}, \quad \gamma = \frac{M}{m_e}, \quad \xi = \frac{d\chi}{d\delta}. \tag{9}$$

In Eqs. (8) and (9), λ_D is the Debye length, ω_p is the plasma frequency (rad/s), ν_{rf} is the frequency of the applied rf voltage, T_e is the electron temperature, m_e is the electron mass, M is the ion mass, and T is the heavy particle temperature. The normalized values are: spatial coordinate, χ; time, δ; frequency, ψ; potential, Φ; electrical field, η; mass, γ; temperature, τ; and velocity, ξ. With these definitions, the ion acceleration transforms as

$$\frac{dv(x,t)}{dt} = \frac{eE(x,t)}{M} \rightarrow \frac{d\xi(\chi,\delta)}{d\delta} = \frac{4\pi^2\eta(\chi,\delta)}{\gamma}. \tag{10}$$

In typical rf discharges used for plasma processing of semiconductors, $T_e \approx 2$–5 eV, and the electron density is in the range 10^9–10^{10} cm^{-3}. The applied rf frequency is in the range of 100 kHz–50 MHz, and the applied rf voltage is tens to hundreds of volts. The sheath thickness is a few millimeters. For these conditions, $\lambda_D \approx 0.1$–0.5 mm, and $\omega_P \approx 1.8$–5.6 GHz. This yields normalized values for the applied rf voltage (Φ_{rf}) of 5–50; normalized frequency (ψ) 10^{-5}–10^{-2}; and normalized sheath thickness (χ_S) of 2–10.

III. RESULTS FOR THE ENERGY AND ANGULAR DISTRIBUTION OF IONS STRIKING THE ELECTRODES

Ions falling through a collisionless dc sheath arrive at the electrode with energies equal to the sheath potential. This monoenergetic distribution differs from the distribution for ions in an rf discharge. Ions falling through an rf sheath arrive at the electrode with a distribution of energies that results from the oscillatory motion of the sheath and the inability of the massive ions to respond in phase to changes in the electric field. The sheath in an rf discharge may oscillate in either space or in magnitude of the potential; that is, the thickness of the sheath may change during an rf cycle, the value of the sheath potential may oscillate, or a combination of the two may occur. As an ion enters an oscillating sheath, it is accelerated by the advancing electric field, and obtains a velocity which it retains while the sheath is in retreat during the second half of the rf cycle. When the sheath next extends into the plasma the ion is again accelerated, and this process continues until the ion strikes the electrode.

A scaling parameter can be obtained to classify the general shapes of the IED for ions striking the electrodes in rf discharges. This scaling parameter S is a measure of the ability of an ion to respond to changes in the electric field within the sheath. An ion is considered able to respond to changes in the electric field if, during one rf cycle, it is accelerated to a sufficient velocity to cross the sheath. This ability is measured by

$$\frac{1}{S} = \frac{1}{l}\frac{eE}{2M}\left(\frac{1}{\nu_{\mathrm{rf}}}\right)^2, \tag{11}$$

where E is the electric field within the sheath. If $S \ll 1$, the ion is able to respond to the electric field. If $S \gg 1$, the ion is unable to respond. In dimensionless form,

$$\frac{\gamma\psi^2\chi_S^2}{\Phi_S} = 2\pi^2 S^2 \equiv \frac{S'}{100}, \tag{12}$$

where we define $\Phi_S = |\Phi_{\mathrm{dc}}| + \Phi_{\mathrm{rf}}$ and $\chi_S = \chi_{\mathrm{dc}} + \chi_{\mathrm{rf}}$. The factor of 100 in Eq. (12) is used merely to rescale S' to a more convenient range. Conditions for which the ion cannot respond to changes in the electric field (i.e., large values of S') correspond to large ion mass, high frequency, thick sheaths, or small sheath potential.

Three regimes for the IED can be identified as a function S'. In Regime 1 ($S' < 2$), the initial increment of velocity obtained by the ion when first acted upon by the advancing sheath is sufficiently large that the ion moves an appreciable distance towards the electrode while the sheath is in retreat. As a result, when the sheath next advances into the plasma and beyond the ion, the ion does not experience the maximum electric field. As a result, the ion strikes the electrode with an energy distributed between the minimum and maximum sheath potential. In Regime 2 ($2 < S' < 500$) the ion remains within the sheath for many rf cycles, and therefore experiences the electric field corresponding to the maximum sheath potential many times. The ion strikes the electrode with an average energy close to that of the maximum sheath potential. Few ions strike the electrodes with an energy close to the minimum sheath potential. In Regime 3 ($S' > 500$) the oscillation of the sheath is sufficiently fast that the ions respond only to the average sheath potential. In this regime, the IED becomes progressively narrower as the ion mass or rf frequency increase.[2,5–7]

A. Ion mass and rf frequency

The dependence of the IED on rf frequency and the mass of the ion is plotted in Figs. 2, 3, and 4. For these figures, the normalized sheath thicknesses and potentials are $\chi_{\mathrm{dc}} = 6$, $\chi_{\mathrm{rf}} = 6$, and $|\Phi_{\mathrm{dc}}| = \Phi_{\mathrm{rf}} = 15$. The exponent in Eq. (3) is $a = 1$, and the sheaths are collisionless. The initial ion temperature is $\tau = 0.025$. The final results are not sensitive to the choice of τ provided that $|\Phi_{\mathrm{dc}}| + \Phi_{\mathrm{rf}} \gg \tau$. In Fig. 2, the IED is plotted for rf frequencies $\psi = 10^{-3}$, 3×10^{-4}, and 10^{-4} for an ion mass of 40 amu ($S' = 35.2$, 3.2, 0.35). In Fig. 3, the rf frequency is constant ($\psi = 2\times10^{-4}$) and the IED is plotted for ion masses of 1, 40, and 130 amu

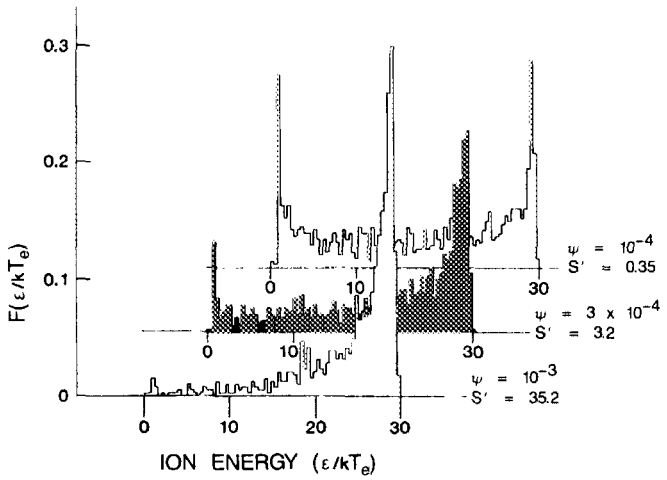

FIG. 2. Ion energy distributions (IED) for an ion of mass 40 amu (argon) for different normalized rf frequencies; $\psi = 1 \times 10^{-3}, 3 \times 10^{-4}$, and 1×10^{-4} ($S' = 35.2$, 3.2, and 0.35). The IED plotted in the background of the figure is typical of a distribution for a small S' (Regime 1). The IED plotted in the foreground is typical of a distribution for intermediate S' (Regime 2).

($S' = 0.035$, 1.40, and 5.47). For conditions where either the rf frequency is small or the ion mass is small (i.e., Regime 1), the ions "track" the motion of the sheath and the IED has a bimodal shape. The flux of ions striking the surface is maximum at an energy corresponding to the extrema of the rf excursion of the sheath potential due to longer time proportionally spent at those values. During the transit of light ions through a sheath oscillating at higher frequencies, the ions experience many rf cycles. The probability is small that an ion traversing the sheath will experience, on the average, the minimum sheath potential. Therefore, the lower energy extrema in the IED is lost and the distribution is maximum at

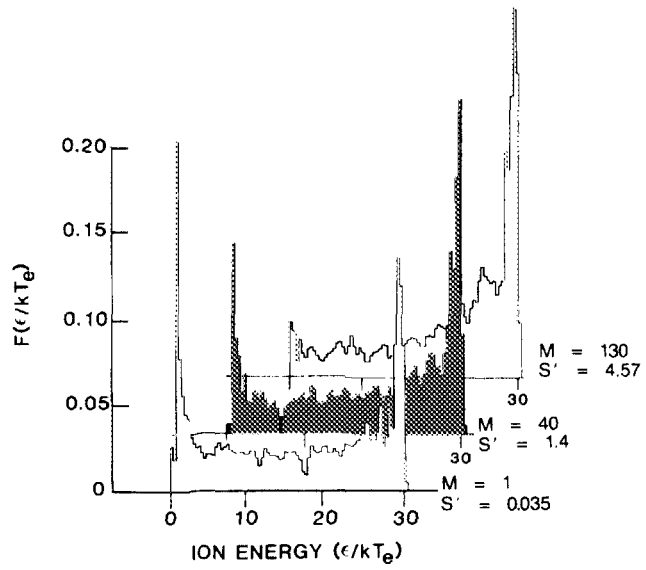

FIG. 3. Ion energy distributions (IED) for a normalized rf frequency of 2×10^{-4} and ion masses of 1, 40, and 130 amu (hydrogen, argon, and xenon). The S' values are 0.035, 1.4, and 4.57. The IED plotted in the foreground of the figure is typical of a distribution for a small S' (Regime 1). The IED plotted in the background is typical of a distribution for intermediate S' (Regime 2).

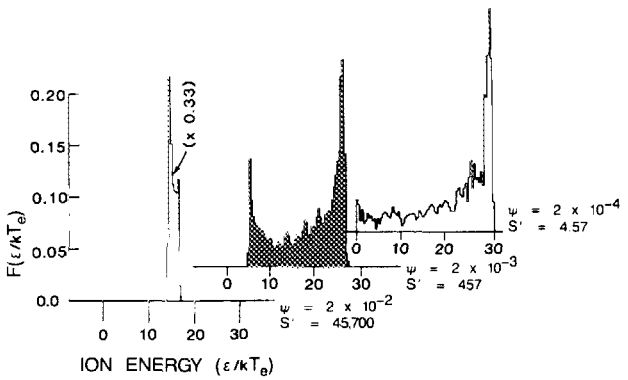

FIG. 4. Ion energy distributions (IED) for an ion of mass 130 amu (xenon) for different normalized rf frequencies; $\psi = 2 \times 10^{-2}$, 2×10^{-3}, and 2×10^{-4} ($S' = 45700$, 457, and 4.57). The IED plotted in the foreground of the figure is typical of a distribution for a large S' (Regime 3). The IED plotted in the background is typical of a distribution for intermediate S' (Regime 2).

the sum of the dc and rf sheath potentials. For these (i.e., Regime 2) conditions, the ions are within the sheath for a larger fraction of their transit to the electrode, and therefore have a higher probability of experiencing the maximum sheath potential. The transition between an IED for intermediate S' (Regime 2) and small S' (Regime 1) is clearly shown in Figs. 2 and 3.

With higher frequencies and heavier ions (large S'), the ions begin to respond only to the average sheath potential. This trend is observed experimentally as a narrowing of the IED centered about the average potential as S' increases.[2,5–7] In those studies the width of the distribution was observed to be proportional to $M^{-1/2}$ provided the transit time of the ion through the sheath is long compared to the rf period. This condition corresponds to large S' (Regime 3). We see this narrowing of the IED in Fig. 4 for ions of 130 amu and frequencies $\psi = 2 \times 10^{-4}, 2 \times 10^{-3}$, and 2×10^{-2} ($S' = 4.57$, 457, and 45700) spanning Regime 2 to Regime 3.

The appropriateness of S' as a scaling parameter is illustrated in Fig. 5. In this figure, the IED is plotted for conditions where the values of γ, ψ, Φ_S, and χ_S are individually varied over a wide range in their respect values, and in such a manner to keep the scaling parameter constant ($S' = 3.2$). The ranges of these parameters are $3.7 \times 10^4 \leqslant \gamma \leqslant 1.5 \times 10^5$ ($20 \leqslant M_{amu} \leqslant 80$); $1 \times 10^{-4} \leqslant \psi \leqslant 9 \times 10^{-4}$; $8 \leqslant \chi_S \leqslant 18$; and $15 \leqslant \Phi_S \leqslant 60$. With the energy scale normalized to the magnitude of Φ_S, the resulting IEDs are very similar in shape, thereby demonstrating that S' is an appropriate scaling parameter for changes in its parameters of the described magnitude.

B. Phase between sheath potential and thickness

The IEDs plotted in Figs. 2–4 are for conditions where both the sheath potential and sheath thickness have dc and rf components, and the potential and thickness are in phase. Similar results are obtained if the sheath potential is as described but the sheath has a constant thickness. The extremum at the maximum of the rf excursion, though, is somewhat more dominant with constant sheath thickness. This results from the fact that in the absence of spatial oscillation,

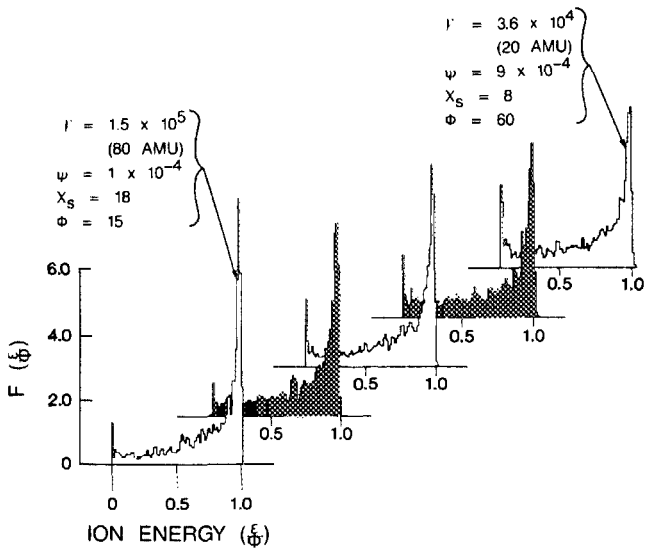

FIG. 5. Ion energy distributions (IED) for constant scaling parameter $S' = 3.2$ while varying γ, ψ, χ_S, and Φ_S. The range of these parameters is $3.7\times10^4<\gamma<1.5\times10^5$ ($20<M_{amu}<80$); $1\times10^{-4}<\psi<9\times10^{-4}$; $8<\chi_S<18$; and $15<\Phi_S<60$. The similarity in the shape of the IED for large variations in these parameters while maintaining S' constant confirms that S' is an appropriate scaling parameter.

once entering the sheath an ion is constantly accelerated. A similar effect is obtained when the exponent a in Eq. (5) is increased, although the changes are not large.

Significant changes in the shape of the IED, though, can occur when the rf components of the sheath potential and thickness are out of phase with each other. The dependence of the IED on the phase of oscillation is shown in Fig. 6 where the IED is plotted for conditions where the rf components of the sheath potential and thickness are in phase ($\alpha = 0$) and π radians out of phase ($\alpha = \pi$). The rf frequency and ion mass are $\psi = 10^{-4}$, $M = 40$ amu ($S' = 0.35$). The sheath properties are otherwise the same as in Fig. 2. The IED for in-phase oscillation has the characteristic shape discussed above for Regime 1. The IED for out-of-phase oscillation has the peak of its distribution at low energy. This change in shape results from the ion spending a larger fraction of its transit within the sheath boundary (i.e., when the sheath is thickest) at a time when the sheath potential is at its minimum value. Also note that for the out-of-phase example it is possible to obtain an energy greater than the sum of the dc and rf potentials. An ion having this energy was accelerated by the sheath when it was at its maximum spatial extent, but minimum potential. Having obtained a sufficiently large velocity, the ion tracks the retreat of the sheath, remaining in an electric field that increases in time as the sheath potential increases. In doing so, the ion may enter the sheath at the time of its retreat (when it is thinnest and has the largest potential) already having gained energy from its previous encounter with the sheath half a cycle before. Changes in the phase of the sheath thickness and sheath potential are seen to distort the shape of the IED and therefore should be considered in the interpretation of experimental data.

C. Collisions

Charge exchange collisions occurring within the sheath are manifested in two ways; the IED is thermalized and the angular distribution of ions (IAD) striking the electrodes is broadened. The IED and IAD for ions as functions of mean-free path for charge exchange collisions are plotted in Figs. 7 and 8. For these results, $M = 40$ amu and $\psi = 10^{-4}$ ($S' = 0.35$). The dc and rf sheath thicknesses are as for Fig. 2. In Fig. 7 IEDs are plotted for mean-free paths between charge exchange collisions, measured in Debye lengths, of 10, 3, 1, and 0.3. These values correspond to mean-free paths as a fraction of the average sheath thickness of 1.67, 0.5, 0.17, and 0.05. For a charge exchange cross section of 50 A^2, this would imply a pressure range of 0.03–1.0 Torr. As the mean-free path decreases, the IED is downshifted in energy, a reflection of the IED beginning to equilibrate with the low-temperature distribution of the neutral gas ($\tau = 0.025$) with

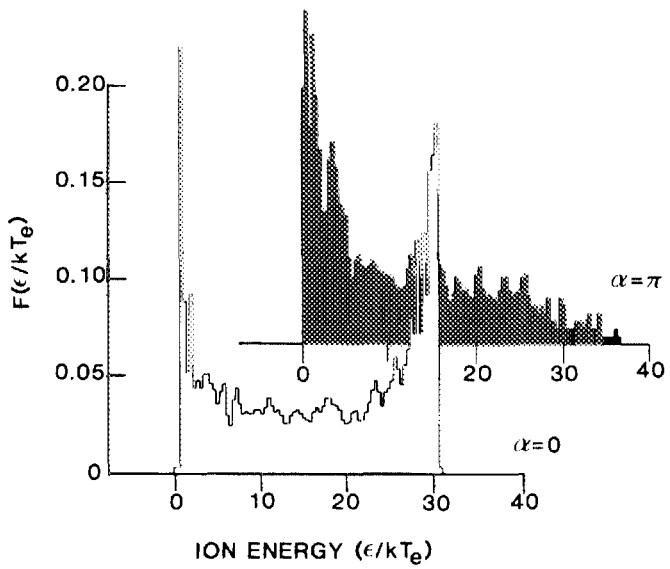

FIG. 6. Ion energy distributions (IED) for an ion of mass 40 amu (argon) and $\psi = 1\times10^{-4}$ ($S' = 0.35$) for in phase ($\alpha = 0$) and out of phase ($\alpha = \pi$) oscillation between the sheath potential and sheath thickness.

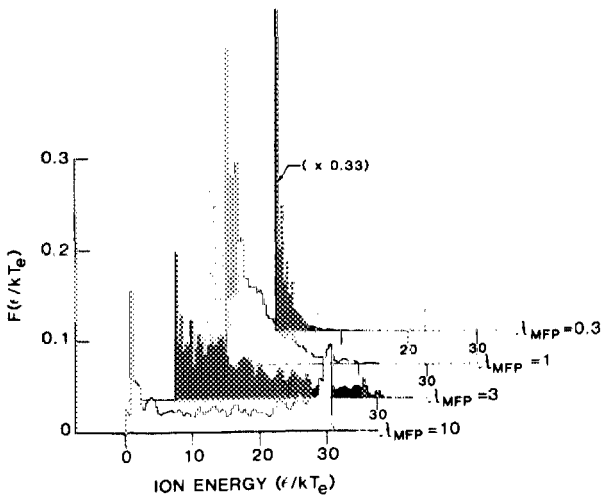

FIG. 7. Ion energy distributions (IED) for an ion of mass 40 amu (argon) and $\psi = 1\times10^{-4}$ ($S' = 0.35$) for different values of the mean-free path for charge exchange collisions (λ_{MFP}). The IEDs plotted are for $\lambda_{MFP} = 10$, 3, 1, and 0.3 Debye lengths. These values correspond to 1.67, 0.5, 0.17, and 0.05 of the average sheath thickness.

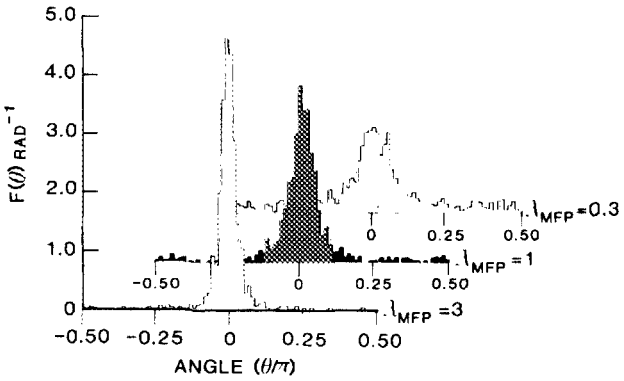

FIG. 8. Ion angle distributions (IAD) for the conditions of Fig. 7. The IADs plotted are for $\lambda_{MFP} = 3$, 1, and 0.3 Debye lengths. These values correspond to 0.5, 0.17, and 0.05 of the average sheath thickness.

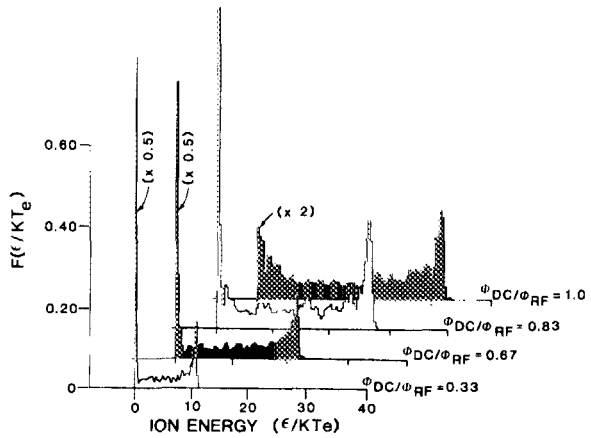

FIG. 9. Ion energy distributions (IED) for an ion of mass 4 amu (helium) and $\psi = 3\times10^{-4}$ for different values of the ratio $|\Phi_{dc}|/\Phi_{rf}$. The IEDs plotted are for $|\Phi_{dc}|/\Phi_{rf} = 0.33, 0.67, 0.8$, and 1.0 ($S' = 0.47, 0.38, 0.35, 0.32$). The sheath model used for this figure is as given by Eq. (13). The IED shifts to lower energy and becomes more thermal as $|\Phi_{dc}|$ decreases.

which it is undergoing charge exchange reactions. Coincident to the degradation in energy of the IED, and IAD spreads in angle away from the vertical, a reflection of the transition from the anisotropic distribution one obtains under collisionless conditions to the random angular distribution of the neutral gas. (See Fig. 8.) The spreading in angle of the IAD has important consequences in plasma etching where an anisotropic delivery of activation energy to the surface is required to obtain vertical etches and to etch features whose depth exceeds their width (see Sec. IV).

D. Φ_{dc}/Φ_{rf}

For the type of electropositive capacitively coupled rf discharges described in Sec. II, the plasma potential usually remains positive with respect to the potential of surfaces emersed in the plasma; that is, sheath potentials are always negative. This condition results from the requirement that surfaces within the plasma cannot continue to collect a net charge during an rf cycle. Because the electrons are many times more mobile than ions and usually have a higher temperature, a negative sheath potential (i.e., positive plasma potential) is required to insure that the random (and directed) flux of electrons collected by a surface is equal to the flux of ions.

When Φ_{dc} is negative and is equal in magnitude to the amplitude of the rf applied voltage, the sheath potential is always negative and the required conditions are satisfied. If Φ_{dc} has a more positive value, the time varying magnitude of the rf sheath potential must decrease or become nonsinusoidal in order to maintain a negative sheath potential. For the condition where $|\Phi_{dc}| < \Phi_{rf}$ two forms for the plasma potential are suggested.[1] The first appears as Eq. (1), and is repeated in Eq. (13), and the second appears in Eq. (14);

$$\phi_P(t) = \mathrm{MAX}(\phi_{dc}^* + \phi_{rf}^* \sin(\omega_{rf} t), \Delta\phi), \tag{13}$$

$$\phi_P(t) = \frac{(\phi_{dc}^* + \phi_{rf}^*)}{2}[1 + \sin(\omega_{rf} t)]. \tag{14}$$

The form in Eq. (13) is for a sheath exhibiting dominantly resistive behavior whereas the form in Eq. (14) is for a sheath exhibiting dominantly capacitive behavior.[1] These plasma potentials, and the corresponding sheath potentials, are shown schematically in Fig. 1.

Using the expression in Eq. (13) for the plasma potential, the IED and IAD for different relative values of Φ_{dc} and Φ_{rf} are plotted in Figs. 9 and 10. For these figures, the sheaths are collisionless, $\psi = 3\times10^{-4}$, $M = 4$ amu, and the maximum normalized sheath thickness is $\chi_S = 10$. The value of Φ_{rf} remains fixed ($\Phi_{rf} = 16.5$) while Φ_{dc} is varied. In Fig. 9, $|\Phi_{dc}|/\Phi_{rf} = 0.33$, 0.67, 0.8, and 1.0 ($S' = 0.47$ to 0.32, respectively). In Fig. 10, these values are 0., 0.33, 0.67, and 1.0. The rf and dc components of the sheath thickness scale with the relative magnitudes of Φ_{rf} and Φ_{dc}, respectively, while maintaining the fixed maximum value. As $|\Phi_{dc}|$ decreases, the IED is both shifted to lower energy and the thermal portion of the IED increases in relative magnitude. The thermal component results from ions diffusing into the sheath when it is thin and when the sheath potential at its minimum value. As $|\Phi_{dc}|$ decreases, the fraction of the rf cycle during which this occurs increases, and hence the thermal component of the IED increases proportionately. The large thermal component of the IED shown here has been observed experimentally for similar conditions where the plasma potential is believed to be at a minimum value for a large fraction of the rf cycle.[3]

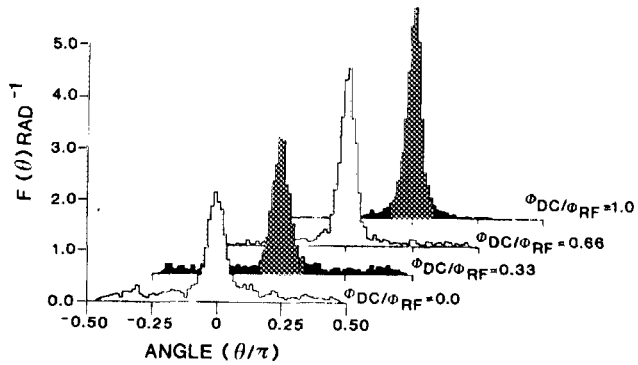

FIG. 10. Ion angle distributions (IAD) for the conditions of Fig. 9. The IADs plotted are for $|\Phi_{dc}|/\Phi_{rf} = 0.$, 0.33, 0.67, and 1.0 ($S' = 0.63$, 0.47, 0.38, 0.32). As $|\Phi_{dc}|$ decreases the IAD broadens.

Concurrent with the thermalization of the IED, the IAD also broadens, a consequence of the random thermal trajectories with which the thermalized ions in the plasma drift into the sheath when the potential is small. This broadening is illustrated in Fig. 10. Recall that the broadening of the IAD for these conditions is important with respect to maintaining the anisotropic etching obtained with plasma etching (see Sec. IV).

Using the expression in Eq. (14) for the plasma potential, the IED is plotted in Fig. 11. for $|\Phi_{dc}|/\Phi_{rf} = 0.33$ and 1.0 ($S' = 0.47$ and 0.32). Conditions are otherwise the same as in Fig. 9. With this form for the potential, the IED shifts to lower energy with decreasing $|\Phi_{dc}|$ however the IED retains its shape and the IAD does not broaden. The shapes of the IED and IAD are therefore a method of discriminating between the two forms of the potential discussed here, and therefore a method for diagnosing whether the sheaths display dominantly capacitive or resistive behavior.

IV. ANISOTROPIC ENHANCEMENT OF ETCHING RATES DUE TO ENERGETIC ION BOMBARDMENT

The rate of etching of semiconductor materials during the plasma etching process proceeds by at least two mechanisms.[10–12] The first is a purely thermally activated or spontaneous chemical etching process intiated by the adsorption of neutral radicals from the plasma onto the surface. These radicals are adsorbed without discrimination with respect to vertical and horizontal surfaces. The etch therefore proceeds in an isotropic manner. The second mechanism is an enhancement in the rate of chemical etching as a result of the surface being bombarded by energetic ions. To the degree that horizontal surface are bombarded at a higher rate than vertical surfaces, the etch rate for horizontal surfaces is larger and the etch is anisotropic.

The details of the mechanisms by which ion bombardment increases the rate of etching are unclear. The energy carried to the surface by ions may be responsible for preparing favorable adsorption sites for neutral radicals by "damaging" the surface, increasing the rate of desorption from the surface of the etching products, reducing the coverage of surface inhibitors by stimulated desorption, or by increasing the rate of the etching by providing an activation energy for the chemical reaction of adsorbed species.[10–12,20–22]

If we assume that for any of the mechanisms listed above the rate of enhancement of the etching process is proportional to the power deposited on the surface by ion bombardment, then we can estimate the influence of ion bombardment on the isotropy of plasma etching. This estimate is obtained from the results of this model by calculating the power deposited by bombarding ions on horizontal surfaces as compared to vertical surfaces. The surface feature we will use for this study is a rectangular well with a ratio of well depth to width of ρ; deep wells have large values of ρ. The relative enhancement of the etching rate of horizontal surfaces as compared to vertical surfaces is obtained by summing the energy of ions which collide with the side walls and floor of the well. The ratio of this value for the floor of the well compared to the value for the walls of the well is the enhancement in the vertical etching rate produced by ion bombardment R_H. The larger this ratio, the higher the degree of anisotropy the etching process will have. In integral form, this ratio is

$$R_H = 2\rho \frac{\int_0^{\theta_c}\int_0^{\infty}(1-\rho\tan\theta)f(\epsilon,\theta)\epsilon\, d\epsilon\, d\theta}{\int_0^{\theta_c}\int_0^{\infty}\rho\tan\theta f(\epsilon,\theta)\epsilon\, d\epsilon\, d\theta}, \tag{15}$$

where θ is the angle of incidence of the ion, as measured from the vertical, ϵ is the ion energy, and $f(\epsilon,\theta)$ is the energy and angular distribution of the incident ions. The critical shadowing angle is $\theta_c = \tan^{-1}(1/\rho)$.

The enhancement ratio for etching horizontal surfaces R_H is plotted in Fig. 12. The conditions are identical to those for Figs. 9 and 10 in which we compared $f(\epsilon,\theta)$ for different values Φ_{dc} and Φ_{rf}. Recall that when $|\Phi_{dc}| < \Phi_{rf}$, the IED is thermalized and the IAD broadens away from the vertical. In Fig. 12, R_H is plotted as a function of the ratio $|\Phi_{dc}|/\Phi_{rf}$

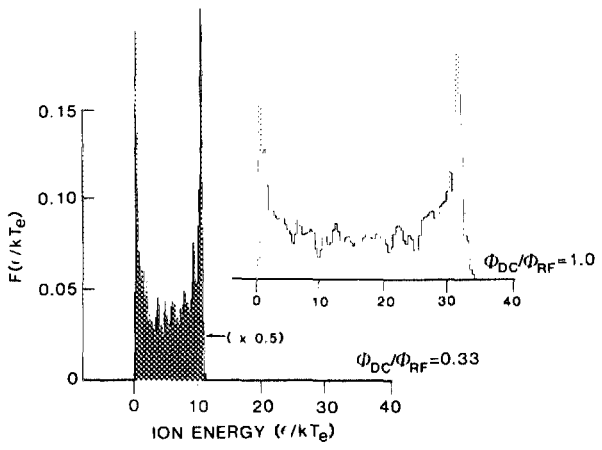

FIG. 11. Ion energy distributions (IED) using Eq. (14) as the sheath model for $|\Phi_{dc}|/\Phi_{rf} = 0.33$ and 1.0 ($S' = 0.47, 0.32$). Conditions are otherwise the same as in Fig. 9. With this model, the IED shifts to lower energy, however, the IED remains symmetric about the average sheath potential.

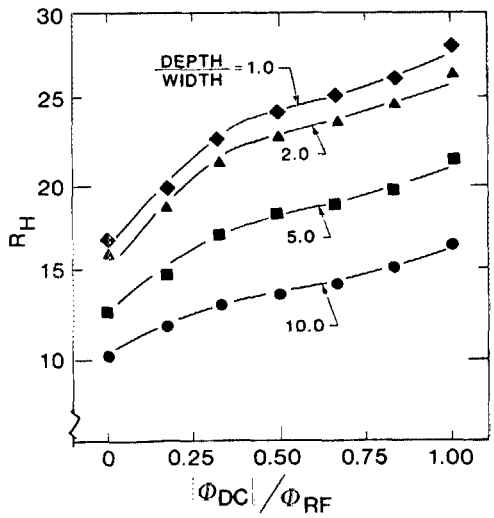

FIG. 12. Ratio of the enhancement in etching rate for horizontal surfaces compared to that for vertical surfaces R_H as a function of $|\Phi_{dc}|/\Phi_{rf}$ for different values of ρ (well depth/width).

for different values of ρ (the ratio of well depth to well width). As $|\Phi_{dc}|/\Phi_{rf}$ decreases so does R_H indicating that the etching process becomes more isotropic. These results are complementary to the experimental results of Zarowin and Horwath.[21] By correlating sheath potential to rf power, they have demonstrated increasing etch anisotropy with increasing sheath potential, and have attributed the effect to the increase in the anisotropy of bombarding ions. Zarowin[22] has also quantified the correlation between etch anisotropy and ion anisotropy by use of an ion energy ellipsoid which describes the directionality of the bombarding ions. Note that R_H is also a function of the ratio of well depth to well width. As the well deepens (i.e., ρ increases) the enhancement for the etching of horizontal surfaces decreases and the anisotropy of the etch decreases. We see that during the plasma etching process as a feature is etched deeper, thereby increasing ρ, the degree of isotropy of the etch increases. Increasingly larger values of ρ require larger values of $|\Phi_{dc}|/\Phi_{rf}$ to maintain a given rate of anisotropic enhancement.

V. CONCLUDING REMARKS

A parametric model for an rf sheath in conjunction with a Monte Carlo model for ion trajectories have been used to compute ion energy distributions (IED) and ion angle distributions (IAD) for ions striking electrode surfaces in an rf discharge. The shape of the distribution can be characterized by the parameter $S' = \gamma\psi^2\chi_S^2/\Phi_S$. For small values of S', the IED is bimodal in shape with energies distributed between the minimum and maximum sheath potential. For large values of S', the IED is centered about the average sheath potential having a width inversely proportional to S'. The IED is significantly perturbed when either collisions occur within the sheath, when $|\Phi_{dc}| < \Phi_{rf}$, or the sheath potential and thickness are out of phase. In the former two cases, the IED shifts to lower energy and becomes more thermal in character. For conditions where $|\Phi_{dc}| < \Phi_{rf}$ the shape of the IED is an indication of the capacitive or resistive nature of the sheaths. Concurrent to the IED shifting to lower energy with collisions or when $|\Phi_{dc}| < \Phi_{rf}$, the IAD broadens away from the vertical. In doing so, the rate of enhancement for plasma etching of horizontal surfaces as compared to vertical surfaces decreases, thereby decreasing the anisotropy of the etching process.

ACKNOWLEDGMENTS

This work was supported by Spectra Technology, Inc., Internal Research and Development funds. The author would like to thank Dr. Richard Roth of Standard Oil Corporate Research Laboratories for his advice and comments on the topic of this paper.

[1] K. Kohler, J. W. Coburn, D. E. Horne, E. Kay, and J. H. Keller, J. Appl. Phys. **57**, 59 (1985).
[2] J. W. Coburn and E. Kay, J. Appl. Phys. **43**, 4965 (1972).
[3] J. W. Coburn and H. F. Winters, Annu. Rev. Mater. Sci. **13**, 91 (1983).
[4] R. T. C. Tsui, Phys. Rev. **168**, 107 (1968).
[5] C. J. Cook, O. Heinz, D. C. Lorents, and J. R. Peterson, Rev. Sci. Instrum. **33**, 649 (1962).
[6] Y. Okamoto and H. Tamagawa, J. Phys. Soc. Jpn. **29**, 187 (1970).
[7] Y. Okamoto and H. Tamagawa, J. Phys. Soc. Jpn. **27**, 270 (1969).
[8] H. R. Koenia and L. I. Maissel, IBM J. Res. Develop. **14**, 168 (1970).
[9] B. Chapman, *Glow Discharge Processing* (Wiley-Interscience, New York, 1980), pp. 143–146.
[10] J. W. Coburn and H. F. Winters, J. Vac. Sci. Technol. **16**, 391 (1979).
[11] V. M. Donnelly, D. L. Flamm, W. C. Dautremont-Smith, and D. J. Werder, J. Appl. Phys. **55**, 242 (1984).
[12] D. L. Flamm, V. M. Donnelly, and D. E. Ibbotson, J. Vac. Sci. Technol. B **1**, 23 (1983).
[13] J. E. Potts, E. M. Peterson, and J. A. McMillan, J. Appl. Phys. **52**, 665 (1981).
[14] K. Ando, M. Aozasa, and R. G. Pyon, Appl. Phys. Lett. **44**, 413 (1984).
[15] A. Matsuda, T. Kaga, H. Tanaka, L. Malhorta, and K. Tanaka, Jpn. J. Appl. Phys. **22**, L115 (1983).
[16] J. C. Knights, R. A. Lujan, M. P. Rosenblum, R. A. Street, and D. K. Bieglesen, Appl. Phys. Lett. **38**, 331 (1981).
[17] M. Mitchner and C. H. Kruger, *Partially Ionized Gases* (Wiley-Interscience, New York, 1973), p. 132.
[18] C. A. Moore, G. P. Davis, and R. A. Gottscho, Phys. Rev. Lett. **52**, 538 (1984).
[19] J. Lucas, Int. J. Electron. **32**, 393 (1972).
[20] H. F. Winters, Materials Research Society 1984 Fall Meeting, Boston, MA., 1984, Paper F1.7.
[21] C. B. Zarowin and R. S. Horwath, J. Electrochem. Soc. **32**, 2541 (1982).
[22] C. B. Zarowin, J. Vac. Sci. Technol. A **2**, 1537 (1984).

Journal of Applied Physics is copyrighted by the American Institute of Physics (AIP). Redistribution of journal material is subject to the AIP online journal license and/or AIP copyright. For more information, see http://ojps.aip.org/japo/japcr/jsp
Copyright of Journal of Applied Physics is the property of American Institute of Physics and its content may not be copied or emailed to multiple sites or posted to a listserv without the copyright holder's express written permission. However, users may print, download, or email articles for individual use.

Journal of Applied Physics is copyrighted by the American Institute of Physics (AIP). Redistribution of journal material is subject to the AIP online journal license and/or AIP copyright. For more information, see http://ojps.aip.org/japo/japcr/jsp